

More uses for Thermal Models

Natasha Sharma¹, Lokesh Kumar² and Sourrendu Gupta³

¹ Department of Physics & Astrophysics, University of Delhi, Delhi 110007, India,

² Department of Physics, Panjab University, Chandigarh 160014, India,

³ International Center for Theoretical Sciences, Tata Institute of Fundamental Research, Survey 151 Shivakote, Hesaraghata Hobli, Bengaluru North 560089, India.

Received: date / Revised version: date

Abstract We explore combinations of particle and anti-particle yields which can be used to test thermal models in a parameter free way. We also explore combinations which can be used to extract μ_B/T , μ_S/T and μ_Q/T . We use experimentally measured particle-antiparticle specific ratios for proton p , Λ , and cascade Ξ , for $\sqrt{s_{NN}} = 7.7\text{--}39\text{ GeV}$ from RHIC BES phase-1 to extract the $\mu_{B,S,Q}/T$. These compared well with published STAR freeze-out parameters. These combinations are verified to predict a similar combination of Ω and $\bar{\Omega}$ yields. We also extend this idea to predict (anti-)nuclei yields at energies where they are not measured. We also update parametrizations for the $\sqrt{s_{NN}}$ dependence of freeze-out parameters T and μ_B , and present for the first time a similar parametrization of μ_S .

PACS. 25.75.Gz, 25.75.Nq, 25.75.Dw, 24.10.Pa

1 Introduction

Relativistic heavy-ion collisions create hot and dense QCD matter whose properties and phase structure are believed to be encoded in final-state hadron abundances. Chemical freeze-out refers to the stage where inelastic collisions cease and particle yields are fixed. The extraction of freeze-out parameters, namely the temperature and chemical potentials (T , μ_B , μ_S , μ_Q), is conventionally performed by global thermal fit to measured hadron yields within statistical hadronization or hadron resonance gas models [1, 2, 3, 4, 5]. These fits depend on hadron lists, decay treatment, and ensemble choice.

An approach we advocate here is to extract parameter ratios $\mu_{B,Q,S}/T$ through experimentally measured particle-antiparticle ratios. These ratios of observables do not involve an overall volume factor nor any masses. They lead to relations that can be analytically inverted, and thereby reduce certain systematic uncertainties. In this paper, we implement this technique on published hadron yields and compare the extracted chemical potential ratios with the results of thermal-model fit obtained by STAR [3] using THERMUS [6]. This approach can also be extended to yields of light nuclei and anti-nuclei. These are the main results presented in this paper.

The paper is organized as follows. Section 2 summarizes the analytic relations used and their inversion. Section 3 describes the data and the analysis choices. A simple test of the approach to thermalization is presented in Section 4. The extracted freeze-out parameters, namely $\mu_{B,Q,S}/T$,

their centrality and energy dependence, and an independent verification, are given in Section 5. In Section 6 the method is extended to light (anti-)nuclei, and implications for fluctuation observables are discussed. Conclusions are presented in Section 7.

2 Using the statistical thermal model

The statistical thermal model assumes that all hadrons follow equilibrium distributions at freeze-out in a high energy collision. Hadron abundances are fixed at chemical freeze-out, defined to be the thermodynamic conditions at which inelastic collisions cease. While the particle spectral distribution offers insight into the kinetic freeze-out conditions where elastic collisions cease. In the grand-canonical (GC) ensemble, the conserved quantities of the system, namely the baryon number B , the strangeness S , and the charge Q , are described by the respective chemical potentials μ_B , μ_S and μ_Q . A fugacity $\lambda_{B,Q,S} = \exp(\mu_{B,Q,S}/T)$ can be defined for each chemical potential, where T is the temperature of the system. The ensemble-averaged density of hadron species i with mass m_i and quantum numbers B_i , S_i and Q_i is

$$n_i(T, \mu_B, \mu_S, \mu_Q) = \frac{g_i}{2\pi^2} m_i^2 T \lambda_B^{B_i} \lambda_S^{S_i} \lambda_Q^{Q_i} K_2\left(\frac{m_i}{T}\right), \quad (1)$$

where, g_i denotes the spin-isospin degeneracy factor and $K_2(x)$ is the second order modified Bessel function. The factor K_2 is obtained for the particles i for which $m_i/T \ll$

1, so the Bose and Fermi distributions are well approximated by the Boltzmann distribution. Practically, at freeze out this is true for all particles except pions. In using these to fit experimentally measured yields, the condition of strangeness neutrality and fixed baryon-to-charge ratio in the initial state are typically used to constrain the chemical potentials μ_S and μ_Q .

For a given hadron species h , the antiparticle \bar{h} , has quantum numbers $B_{\bar{h}} = -B_h$, $Q_{\bar{h}} = -Q_h$ and $S_{\bar{h}} = -S_h$. Eq. (1) then gives the ratio of particle and anti-particle densities as a simple function

$$\begin{aligned} \frac{n_h}{n_{\bar{h}}} &= \lambda_B^{2B_h} \lambda_S^{2S_h} \lambda_Q^{2Q_h} \\ &= \exp \left[\frac{2(B_h \mu_B + S_h \mu_S + Q_h \mu_Q)}{T} \right]. \end{aligned} \quad (2)$$

This is computationally simpler than Eq. (1), since the complicated dependence on the mass cancels out.

Some double ratios are even simpler. For example, we find that

$$\frac{(n_A/n_{\bar{A}})}{(n_p/n_{\bar{p}})} \approx \frac{(n_{\Xi}/n_{\bar{\Xi}})}{(n_A/n_{\bar{A}})} \approx \frac{n_{K^-}}{n_{K^+}} = \exp \left[\frac{4\mu_S}{T} \right], \quad (3)$$

since μ_B/T cancels between the numerator and denominator in the first two, and the approximation involved is that μ_Q/T is small. Such (approximate) equalities of double ratios are checks of local thermal equilibrium that are easily performed before fitting.

Higher cumulants of the distribution probe thermalization even more intensively [7]. These higher order susceptibilities, χ^n (for $n \geq 2$), are constructed experimentally by examining the fluctuations of individual baryons, which we can denote as χ_h^n . In the Boltzmann limit, relations similar to Eq. (3) hold for all these χ_h^n . One finds

$$\frac{\left(\chi_A^n/\chi_{\bar{A}}^n\right)}{\left(\chi_p^n/\chi_{\bar{p}}^n\right)} \approx \frac{\left(\chi_{\Xi}^n/\chi_{\bar{\Xi}}^n\right)}{\left(\chi_A^n/\chi_{\bar{A}}^n\right)} \approx \frac{n_{K^-}}{n_{K^+}}, \quad (4)$$

where μ_Q/T . Higher cumulants of the baryon distribution were found to raise questions about complete thermalization at lower energies in BES-I [8]. In view of this, we anticipate that tests such as those in Eq. (4) will become very important for forthcoming experiments with high intensity and very low beam energies, where χ_A^n and χ_{Ξ}^n may be measured. We emphasize that the double ratios of cumulants of all orders are equal to the ratio n_{K^-}/n_{K^+} in the Boltzmann limit.

Using Eq. (1) one finds that the ratio (R_h) of the arithmetic and geometric means of n_h and $n_{\bar{h}}$

$$\begin{aligned} R_h &\equiv \frac{n_h + n_{\bar{h}}}{2\sqrt{n_h n_{\bar{h}}}} = \frac{1}{2} \left(\sqrt{\frac{n_h}{n_{\bar{h}}}} + \sqrt{\frac{n_{\bar{h}}}{n_h}} \right) \\ &= \cosh \left(\frac{B_h \mu_B + S_h \mu_S + Q_h \mu_Q}{T} \right). \end{aligned} \quad (5)$$

The quantity R_h depends only on the quantum numbers B_h , S_h , Q_h and the chemical potentials, independent of the mass and degeneracy factors. For protons p , Λ , cascade baryons Ξ , and Ω one can write

$$R_p = \cosh \left(\frac{\mu_B + \mu_Q}{T} \right), \quad (6)$$

$$R_{\Lambda} = \cosh \left(\frac{\mu_B - \mu_S}{T} \right), \quad (7)$$

$$R_{\Xi} = \cosh \left(\frac{\mu_B - 2\mu_S + \mu_Q}{T} \right), \quad (8)$$

$$R_{\Omega} = \cosh \left(\frac{\mu_B - 3\mu_S + \mu_Q}{T} \right). \quad (9)$$

Any three of these can be inverted to find the three μ/T ratios. We choose to use Eqs. (6–8) along with experimentally measured yields of p , Λ and Ξ , and leave R_{Ω} as a check. This choice is prompted by the fact that the yields of Ω and $\bar{\Omega}$ are very small because of their larger masses, and hence the measurements come with larger relative uncertainties.

Inverting the above equations gives the expressions

$$\frac{\mu_B}{T} = \frac{1}{2} [\cosh^{-1}(R_p) - \cosh^{-1}(R_{\Xi})] + \cosh^{-1}(R_{\Lambda}), \quad (10)$$

$$\frac{\mu_Q}{T} = \frac{1}{2} [\cosh^{-1}(R_p) + \cosh^{-1}(R_{\Xi})] - \cosh^{-1}(R_{\Lambda}), \quad (11)$$

$$\frac{\mu_S}{T} = \frac{1}{2} [\cosh^{-1}(R_p) - \cosh^{-1}(R_{\Xi})]. \quad (12)$$

The uncertainties in R_p , R_{Λ} , R_{Ξ} propagate to $\frac{\mu_B}{T}$, $\frac{\mu_Q}{T}$, and $\frac{\mu_S}{T}$ using standard linear error propagation.

At LHC energies, these fugacities are close to unity, so particles and anti-particles are produced in equal abundance and particle to anti-particle ratios are unity. On the other hand, data from the STAR collaboration probe a range of values of the fugacities, and so provide us with a non-trivial opportunity to check the validity of Eq. 3. In this context, note that in the published results [3], μ_Q is small and is often taken to be zero. However, in our method, we retain μ_Q as an extracted parameter.

3 Data and analysis details

This work employs identified hadron yields from the STAR for various collision energies and centralities [3]. For each beam energy and centrality bin, we computed R_p , R_{Λ} , R_{Ξ} using Eqs. (6–8) using the published mid-rapidity yields. For energy dependence, the published particle yields from AGS [9, 10, 11, 12, 13] and SPS [14, 15] experiments are also used.

Key systematic considerations include feed-down corrections (particularly for protons), acceptance and efficiency

differences between particles and antiparticles. Double ratios mitigate some, but not all, of these uncertainties. At low energy, baryon stopping changes the composition at mid-rapidity. This must be treated carefully when comparing to global fits. Most of these considerations have been taken into account in the results published by the experimental collaborations. However, corrections due to the weak-decay feed-down for protons still need to be performed. for STAR's p and \bar{p} at were obtained using the THERMUS code [6]. The ratios are computed using central values of measured yields, while the uncertainties on the ratios are evaluated by standard error propagation assuming uncorrelated errors.

4 Test of thermalization

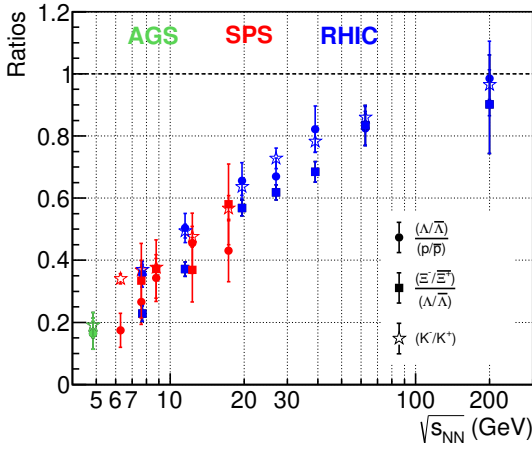


Figure 1: Double ratios of various particles as given in Eq. (3) displayed as functions of the energy $\sqrt{s_{NN}}$.

We start by testing the validity of a statistical hadronization model using Eq. (3) in the various collision energies studied. As we discussed in Section 2, this gives a test of the applicability of the model which does not depend on the specific values of its parameters, except that μ_Q/T is small. The ratios are constructed using experimentally measured particle yields in AGS [9, 10, 11, 12, 13], SPS [14, 15] and RHIC [3, 16]. With these input data, we constructed each of the double ratios given in Eq. (3).

Figure 1 shows the double ratios constructed using p , Λ , Ξ , and K as functions of energy. All of these ratios are consistent with each other within uncertainties at higher energy. However, there could be some deviations from equality at lower $\sqrt{s_{NN}}$. With this caveat, the data suggest that, to a good approximation, these particles are thermally produced in high energy heavy-ion collisions with negligible μ_Q/T . The shape of the curve is a reflection of the change of μ_S/T with $\sqrt{s_{NN}}$. At very high energies ($\sqrt{s_{NN}} \geq 200$

GeV), all the ratios approach unity, reflecting the fact that μ_S/T becomes small.

The ratios presented here include uncertainties obtained by standard error propagation of the published experimental yields. This could lead to overestimates of the uncertainties shown in Figure 1. In future experiments or data analyses, individual sources of systematic uncertainty could be minimized by directly estimating the experimental uncertainties on the particle-antiparticle ratios. This would lead to the cancellation of correlated systematic effects to a large extent. A more precise estimation of these uncertainties would provide stringent tests of thermalization through the double ratios, especially in future high statistics experiments at low energy, starting from BES-II.

5 Results

5.1 Centrality dependence of chemical potential ratios

We have extracted $\mu_{B,S,Q}/T$ ratios at chemical freeze out as functions of number of participant nucleons ($\langle N_{\text{part}} \rangle$) using Eqs. (10)–(12) for gold-on-gold (Au+Au) collisions at $\sqrt{s_{NN}}$ of 7.7, 11.5, 19.6, 27 and 39 GeV. The results obtained are shown in Figure 2.

The fits show that the μ_B/T ratio increases with $\langle N_{\text{part}} \rangle$. This correctly reflects increasing baryon density in more central collisions. The consistent decrease in this ratio with increasing beam energy is consistent with the idea that baryon stopping decreases with increasing collision energy. The μ_S/T ratio is independent of $\langle N_{\text{part}} \rangle$, as expected, since the participants have a fixed strangeness. Observe the significant decrease of μ_S/T with beam energy, where more strange particles are expected to be created at higher energy. This is consistent with the OZI rule, which implies that strange and anti-strange particles are created together. The quantity μ_Q/T is small and therefore has large relative errors, so any statement about trends is necessarily weak.

The smallness of μ_Q/T is related to the fact that the systems are nearly isoscalar. It has a tendency to become more negative with increasing $\langle N_{\text{part}} \rangle$. The Gell-Mann-Nishijima relation, $Q = I_3 + (B + S)/2$ allows us to understand this trend, since increasing the number of participants involves increasing the number of baryons in the system. Similarly, the observation that μ_Q/T moves closer to zero with increasing beam energy has to do with the fact that baryon stopping decreases with energy. In the future, it may be interesting to extract the chemical potential associated with the isospin component I_3 . This is also the parameter used in lattice computations, so this change may be useful direct in comparisons with QCD.

In Figure 3 we show the μ_B/T and μ_S/T ratios as a function of $\langle N_{\text{part}} \rangle$ at the four energies 7.7, 19.6, 27 and 39 GeV. The filled symbols represent the published freeze-out parameter ratios [3], while the solid symbols show the results of this fit. The good agreement between our results

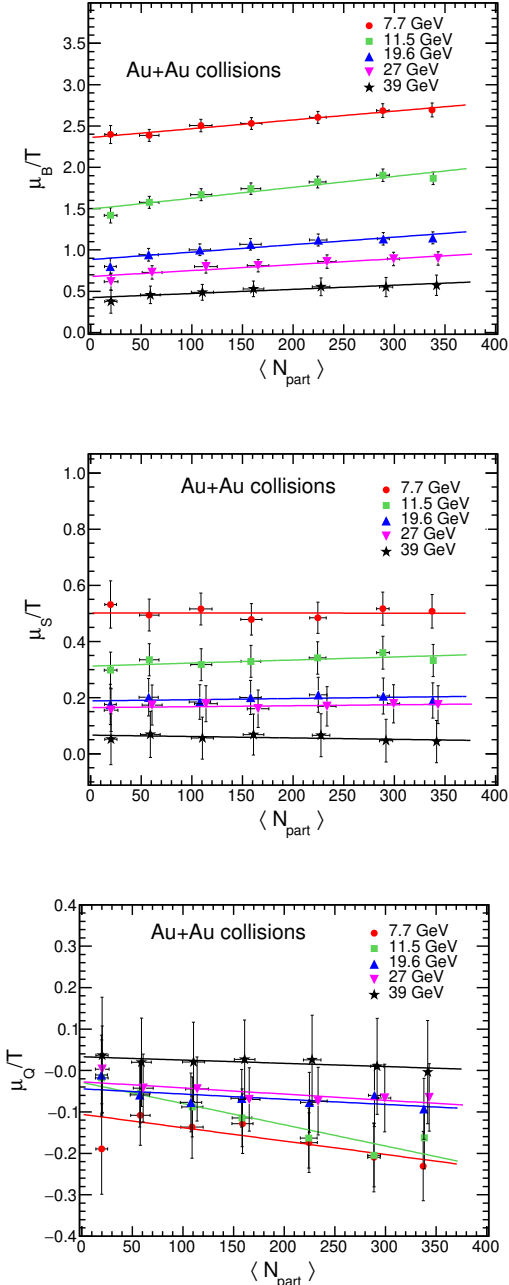


Figure 2: Extracted μ_B/T , μ_S/T , and μ_Q/T ratios as a function of number of participating nucleons $\langle N_{\text{part}} \rangle$ in various energies. Lines represent the linear fits to the data points.

and the published fits from the STAR experiment is a validation of the method used here. Due to the larger relative errors on μ_Q/T , its comparison does not add anything to this conclusion.

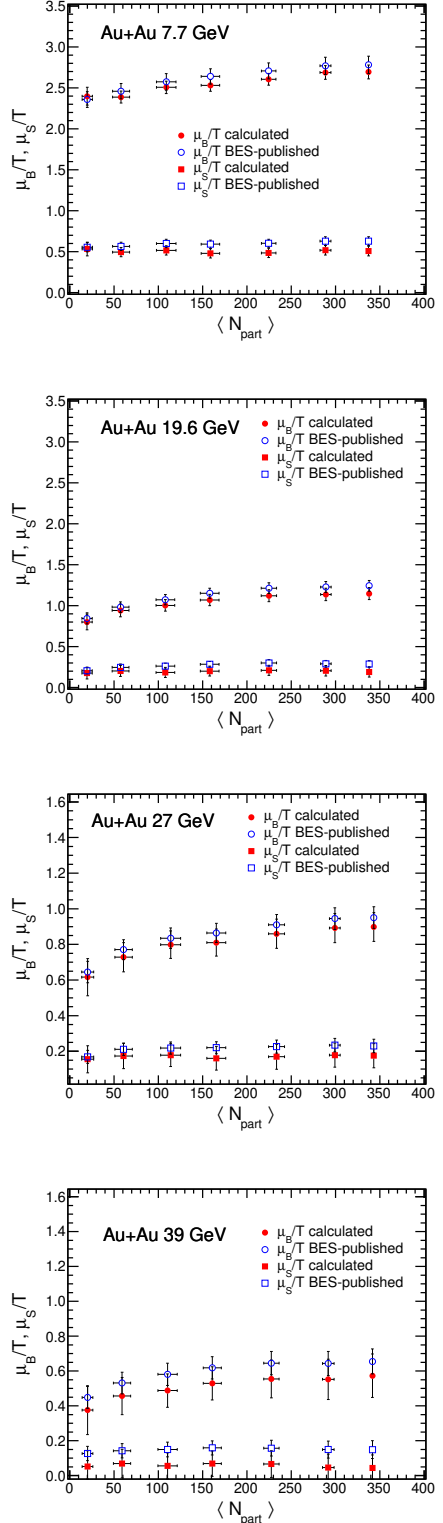


Figure 3: Extracted μ_B/T and μ_S/T ratios at different energies and their comparison with the published freeze-out parameters [3].

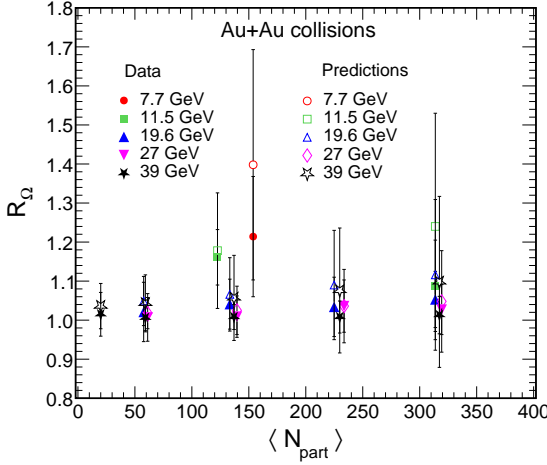


Figure 4: Verification of R_Ω predicted by Eq. (9). The quantity is computed from experimentally measured Ω^- and Ω^+ yields, while the cosh is obtained using the chemical potential ratios obtained using Eqs. (6–8).

5.2 Validation using R_Ω

As mentioned above, R_Ω provides a validation of the method. The experimentally measured Ω^- and Ω^+ yields are used to estimate R_Ω . Using the extracted values of μ_B/T , μ_S/T and μ_Q/T one obtains model predictions for this quantity using Eq. (9). The uncertainties in R_Ω (data) are evaluated using the standard error propagation from the uncertainties in the measured hadron yields, as described in Eq. 5. For the predicted R_Ω , the uncertainties are obtained by propagating the uncertainties in the estimated μ_B/T , μ_S/T and μ_Q/T .

Figure 4 shows this comparison by plotting R_Ω obtained from experiments along with the value predicted by Eq. (9). The two are shown as functions of $\langle N_{\text{part}} \rangle$ in Au+Au collisions at $\sqrt{s_{\text{NN}}} = 7.7, 11.5, 19.6, 27$ and 39 GeV. The complete consistency of the measurements and predictions is a nontrivial validation of Eq. (9). This test is even more interesting since Ω is a multi-strange baryon and so is more sensitive to μ_S/T than any of the inputs.

5.3 Energy dependence of R_p , R_Λ and R_Ξ

Next, we present the energy dependence of R_p , R_Λ , and R_Ξ . The measured values are taken from AGS [9, 10, 11, 12, 13], SPS [14, 15] and RHIC [3, 16]. As mentioned above, the reported yields of p and \bar{p} from STAR were corrected for feed down using THERMUS. The good continuity with the AGS and SPS data shown in Figure 5 suggests that this correction is reliable.

The figure also shows a comparison of the data with the model predictions from Eqs. (6–8), as functions of the collision energy. The values of μ/T are extracted from STAR

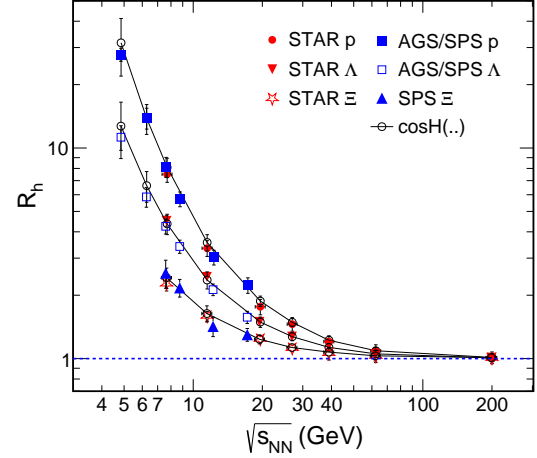


Figure 5: Energy dependence of ratios R_p , R_Λ , and R_Ξ obtained from published hadron yields [9, 10, 11, 12, 13, 14, 15, 3, 16]. Measurements (plotted as points) are compared with model predictions (the smooth curves) obtained using Eqs. (6–8).

data. So are only available at the energies where the data was taken. The continuous curves are obtained using an interpolating formula. We discuss this in the next subsection.

Observe that p , Λ , and Ξ are different at lower energies, but move towards the universal value of unity with increasing energy. This indicates that the ratios μ/T decrease rapidly with increasing energy. The differences between p , Λ , and Ξ can be attributed to μ_S/T . This does not enter R_p , but for Ξ its effect is the square of what it is for Λ . This is visible on the log-log plot at every collision energy, as the vertical displacement between R_p and R_Λ is the same as between R_Λ and R_Ξ .

5.4 Energy extrapolations of freeze-out parameters

The beam energy dependence of the freeze-out parameters has been parametrized before by many authors [17, 18, 19, 20]. We present an update using thermal model fits from STAR BES-I data at $\sqrt{s_{\text{NN}}} = 7.7 - 200$ GeV. The availability of inputs over a larger range of $\sqrt{s_{\text{NN}}}$ than was available earlier helps to better constrain extrapolations. The input freeze out parameters were obtained using the yields of π , K , p , Λ , Ξ , and their antiparticles [3]. The STAR experiment provides good estimates of the particle and antiparticle yields even at lower energies, where the yields are low. In contrast, at AGS and SPS energies, yields of multi-strange hadrons and their antiparticles are seldom reported. As a result, the energy-dependent fits provide good estimates of the chemical potentials at lower AGS and SPS energies.

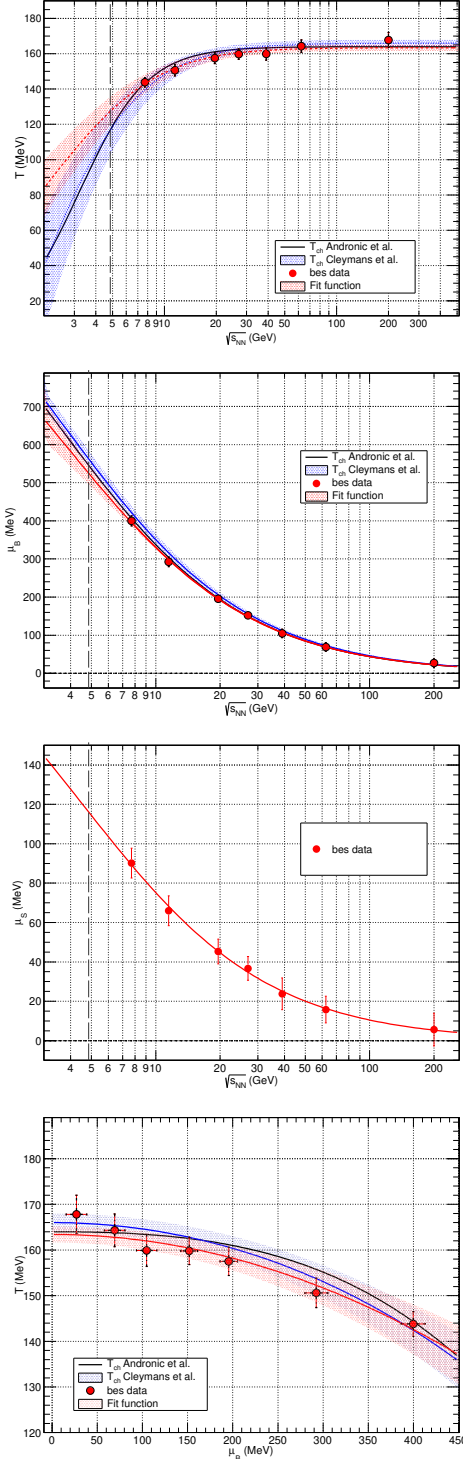


Figure 6: Energy dependence of freeze-out parameters T (top panel), μ_B (second panel), and μ_S (third panel from top). The panel at the bottom shows the freeze-out curve, i.e., T plotted against μ_B . The gray dashed vertical line at $\sqrt{s_{NN}} = 4.85$ GeV marks the lowest energy for which T , μ_B , and μ_S are extracted from data.

Figure 6 shows the energy dependence of freeze-out parameters T , μ_B , and μ_S , as well as T_{ch} versus μ_B and fits to them using the following functional forms

$$T = A - B\mu_B^2, \quad (13)$$

$$\mu_B = \frac{C}{1 + D\sqrt{s_{NN}}}, \quad (14)$$

$$\mu_S = \frac{E}{1 + F\sqrt{s_{NN}}}. \quad (15)$$

Using as input the freeze-out parameters from [3], we find that

$$A = 163.4 \pm 1.8 \text{ MeV} \quad B = (1.3 \pm 0.2) \times 10^{-4} \text{ MeV}^{-1}$$

$$C = 1187 \pm 220 \text{ MeV} \quad D = 0.259 \pm 0.063 \text{ MeV}^{-1}$$

$$E = 239 \pm 104 \text{ MeV} \quad F = 0.218 \pm 0.131 \text{ MeV}^{-1}$$

Table 1 shows the extrapolated values at selected energies.

Table 1: Extrapolated freeze-out parameters corresponding to collision energies at AGS (4.85 GeV), SPS (6.27 GeV), and RHIC (14.5 GeV).

$\sqrt{s_{NN}}$ (GeV)	T_{ch} (MeV)	μ_B (MeV)	μ_S (MeV)
4.85	127.0 ± 6.5	526.4 ± 27.9	116.2 ± 15.6
6.27	136.4 ± 3.9	452.7 ± 17.9	101.0 ± 10.2
14.5	154.9 ± 1.8	249.8 ± 5.7	57.5 ± 3.5

For $\sqrt{s_{NN}} = 14.5$ GeV STAR has taken data [21], but the freeze-out parameters are not yet published, so the parameters given here are reported as the first estimation of chemical freeze-out parameters at this energy. In addition, the energy dependence of μ_S is reported first time along with its functional form and fit parameters.

6 Extension to light nuclei and anti-nuclei prediction

The production mechanism of light nuclei like deuterons (d), tritons (t), ^3He and the corresponding anti-nuclei in high energy collisions is not fully understood. Coalescence models suggest that nuclei and anti-nuclei form when the constituent nucleons lie close in phase space in the final stages of evolution of the system. This formation mechanism is also justified by the small binding energy (\sim few MeV) of (anti-)nuclei compared to the freeze-out temperature (~ 150 MeV) of the system. If the coalescing nucleons are thermal and the coalescence process does not change momenta appreciably, then their experimentally measured densities ratio should satisfy Eq. (5) derived from the simple approximation of the statistical hadronization model [19, 22].

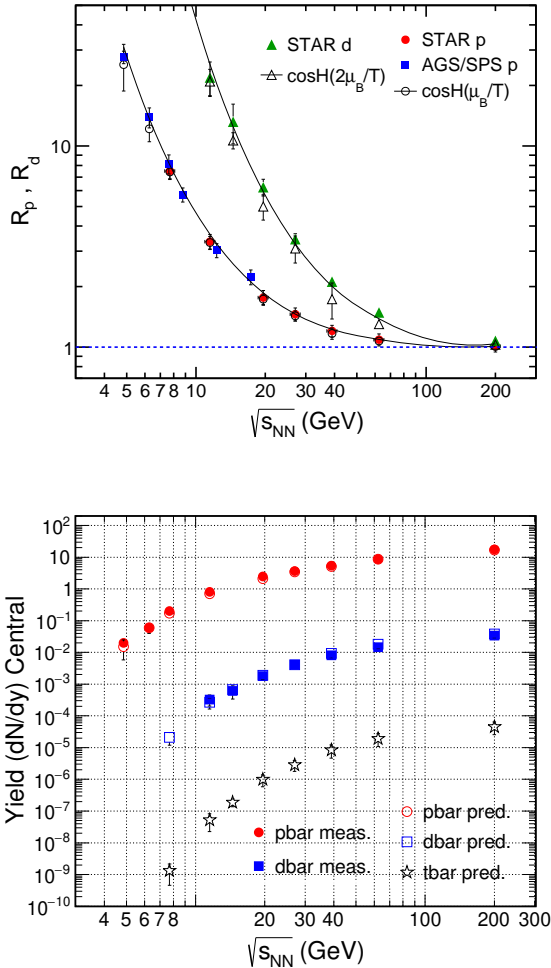


Figure 7: Top: Ratios R_p and R_d , and their comparison with model predictions using μ_B/T as per Eqs. (6) and (16). Bottom: Prediction of anti-nuclei \bar{p} , \bar{d} , and \bar{t} using measurements of nuclei and Eqs. (6), (16), and (17) as explained in the text. Unfilled symbols represent the predictions while the solid symbols represent the published measured yields.

For deuterons ($B_d = 2$) and tritons ($B_t = 3$), Eq. (5) can be written as

$$R_d \equiv \frac{n_d + n_{\bar{d}}}{2\sqrt{n_d n_{\bar{d}}}} \approx \cosh\left(\frac{2\mu_B}{T}\right), \quad (16)$$

$$R_t \equiv \frac{n_t + n_{\bar{t}}}{2\sqrt{n_t n_{\bar{t}}}} \approx \cosh\left(\frac{3\mu_B}{T}\right). \quad (17)$$

We have neglected μ_Q/T because it is very small compared to μ_B/T .

The upper panel of Fig. 7 shows R_p and R_d as functions of $\sqrt{s_{NN}}$. The solid symbols represent values determined using measured experimental yields. The unfilled symbols represent predictions using the values of μ_B/T in Section

5.1, while the smooth lines represent predictions using the values of μ_B/T from [3].

It is observed that R_p and R_d approach unity with increasing energy, since μ/T decreases rapidly with increasing $\sqrt{s_{NN}}$ for reasons that we have discussed in Section 5.1. For any given energy, the ratio deviates further from unity the more baryons it has, as shown in Eqs. (16) and (17).

Since Eqs. (6) and (16) seem to work well, one can invert these equations and use the measured yields of nuclei to give predictions of anti-nuclei yields where measurements are absent or statistically limited. We compare these model predictions with direct measurements of yields in the bottom plot of Figure 7. The predicted anti-proton and anti-deuteron yields agree well with the experimental measurements, as is to be expected from the panel above that. Note that \bar{d} yields are not available at $\sqrt{s_{NN}} = 7.7$ GeV, so the value given in the figure is a true prediction. We have also given a similar prediction for \bar{t} using Eq. (17) and measurements of tritons. These are also genuine predictions of the model and can be tested in the future.

7 Conclusions

Double ratios of particle and antiparticle yields have a very simple form in thermal models, as shown in Eq. (3), when the particle mass is much larger than T and μ_Q/T is small. This makes the equality of certain double ratios into simple tests of thermal models. We demonstrate such a test in Figure 1. Clearly, quick tests such as this, or ones involving susceptibilities, as in Eq. (4), would be important as heavy-ion collision energies are further lowered in the future.

We build a different variable, R_h defined in Eq. (5), which can be used to extract $\mu_{B,S,Q}/T$ with minimal computational work. We demonstrate the use of such an approach by showing the extraction of μ_Q/T using BES-I data from STAR. The data already show certain interesting trends with varying N_{part} and $\sqrt{s_{NN}}$. Certainly, using BES-II data will give better control on the errors in this determination purely through the increased statistics. Furthermore, at lower energy and higher event rates, one can envisage a more detailed study of μ_Q/S . This could have implications on the extrapolation of heavy-ion data to neutron stars, especially when μ_Q is traded for the isospin chemical potential.

We have demonstrated that this method agrees with the results of the fits reported by STAR using the same input data. We also verified that the method correctly predicts R_Q . We also presented a parametrization for the change of T , μ_B , and μ_S with $\sqrt{s_{NN}}$. For μ_S , this is the first time that the energy dependence has been parametrized. These parameters allow us to predict the T , μ_B , and μ_S at lower energies (AGS, SPS and below) and at energies

where they are not yet estimated in BES (for example, at $\sqrt{s_{NN}} = 14.5$ GeV).

The use of the variable R_h , defined in Eq. (5), also extends naturally to light (anti-)nuclei. This extension is agnostic to whether these bound states are created by statistical hadronization or a coalescence mechanism, as we argued in Section 6. We tested this idea using R_d constructed from deuteron and anti-deuteron yields. Then we inverted this argument to predict the anti-deuteron yield at $\sqrt{s_{NN}} = 7.7$ GeV, where it has not yet been reported. We also used this method to predict anti-tritium yields across a range of energies. This could be tested in the future.

In exploring the phase diagram of QCD, the focus has moved to regions with high μ_B and low T . This is the domain of experiments with low beam energy and high statistics. At the same time, μ_S and μ_Q are also needed with precision so that the knowledge gleaned from heavy-ion collisions can be extrapolated to neutron stars. We have demonstrated that building new combinations of experimental observables can explore more details than global fits have revealed in the past.

Acknowledgements

The authors thank S. Chatterjee for interesting and useful discussions. L.K. acknowledges the financial support from Research Grant No. SR/MF/PS-02/2021-PU (E-37120) of the Department of Science and Technology, Government of India. N.S. acknowledges the support from DU-IOE grant Ref. No./IoE/2025-26/12/FRP.

References

1. P. Braun-Munzinger, K. Redlich, J. Stachel, Particle production in heavy ion collisions (2003) 491–599 [arXiv:nucl-th/0304013](https://arxiv.org/abs/nucl-th/0304013), doi:10.1142/9789812795533_0008.
2. A. Andronic, P. Braun-Munzinger, J. Stachel, Hadron production in central nucleus-nucleus collisions at chemical freeze-out, *Nucl. Phys. A* 772 (2006) 167–199. [arXiv:nucl-th/0511071](https://arxiv.org/abs/nucl-th/0511071), doi:10.1016/j.nuclphysa.2006.03.012.
3. L. Adamczyk, et al., Bulk Properties of the Medium Produced in Relativistic Heavy-Ion Collisions from the Beam Energy Scan Program, *Phys. Rev. C* 96 (4) (2017) 044904. [arXiv:1701.07065](https://arxiv.org/abs/1701.07065), doi:10.1103/PhysRevC.96.044904.
4. N. Sharma, J. Cleymans, B. Hippolyte, M. Paradza, A Comparison of p-p, p-Pb, Pb-Pb Collisions in the Thermal Model: Multiplicity Dependence of Thermal Parameters, *Phys. Rev. C* 99 (4) (2019) 044914. [arXiv:1811.00399](https://arxiv.org/abs/1811.00399), doi:10.1103/PhysRevC.99.044914.
5. N. Sharma, J. Cleymans, L. Kumar, Thermal model description of p-Pb collisions at $\sqrt{s_{NN}} = 5.02$ TeV, *Eur. Phys. J. C* 78 (4) (2018) 288. [arXiv:1802.07972](https://arxiv.org/abs/1802.07972), doi:10.1140/epjc/s10052-018-5767-3.
6. S. Wheaton, J. Cleymans, THERMUS: A Thermal model package for ROOT, *Comput. Phys. Commun.* 180 (2009) 84–106. [arXiv:hep-ph/0407174](https://arxiv.org/abs/hep-ph/0407174), doi:10.1016/j.cpc.2008.08.001.
7. D. K. Mark, F. Surace, A. Elben, A. L. Shaw, J. Choi, G. Refael, M. Endres, S. Choi, Maximum Entropy Principle in Deep Thermalization and in Hilbert-Space Ergodicity, *Phys. Rev. X* 14 (4) (2024) 041051. [arXiv:2403.11970](https://arxiv.org/abs/2403.11970), doi:10.1103/PhysRevX.14.041051.
8. S. Gupta, D. Mallick, D. K. Mishra, B. Mohanty, N. Xu, Limits of thermalization in relativistic heavy ion collisions, *Phys. Lett. B* 829 (2022) 137021. doi:10.1016/j.physletb.2022.137021.
9. L. Ahle, et al., Particle production at high baryon density in central Au+Au reactions at 11.6A GeV/c, *Phys. Rev. C* 57 (2) (1998) R466–R470. doi:10.1103/PhysRevC.57.R466.
10. S. Ahmad, et al., Lambda production by 11.6-A/GeV/c Au beam on Au target, *Phys. Lett. B* 382 (1996) 35–39, [Erratum: *Phys.Lett.B* 386, 496–496 (1996)]. doi:10.1016/0370-2693(96)00642-9.
11. S. Albergo, et al., Lambda spectra in 11.6-A-GeV/c Au Au collisions, *Phys. Rev. Lett.* 88 (2002) 062301. doi:10.1103/PhysRevLett.88.062301.
12. S. Ahmad, B. E. Bonner, S. V. Efremov, G. S. Mutchler, E. D. Platner, H. W. Themann, Nuclear matter expansion parameters from the measurement of differential multiplicities for lambda production in central au+au collisions at ags, *Nucl. Phys. A* 636 (1998) 507–524. [arXiv:nucl-ex/9803006](https://arxiv.org/abs/nucl-ex/9803006), doi:10.1016/S0375-9474(98)00218-8.
13. B. B. Back, et al., Anti-lambda production in Au+Au collisions at 11.7-AGeV/c, *Phys. Rev. Lett.* 87 (2001) 242301. [arXiv:nucl-ex/0101008](https://arxiv.org/abs/nucl-ex/0101008), doi:10.1103/PhysRevLett.87.242301.
14. C. Alt, et al., Energy and centrality dependence of anti-p and p production and the anti-Lambda/anti-p ratio in Pb+Pb collisions between 20/A-GeV and 158/A-Gev, *Phys. Rev. C* 73 (2006) 044910. doi:10.1103/PhysRevC.73.044910.
15. C. Alt, et al., Energy dependence of Lambda and Xi production in central Pb+Pb collisions at A-20, A-30, A-40, A-80, and A-158 GeV measured at the CERN Super Proton Synchrotron, *Phys. Rev. C* 78 (2008) 034918. [arXiv:0804.3770](https://arxiv.org/abs/0804.3770), doi:10.1103/PhysRevC.78.034918.
16. B. Abelev, et al., Systematic Measurements of Identified Particle Spectra in pp, d^+ Au and Au+Au Collisions from STAR, *Phys. Rev. C* 79 (2009) 034909. [arXiv:0808.2041](https://arxiv.org/abs/0808.2041), doi:10.1103/PhysRevC.79.034909.
17. J. Cleymans, H. Oeschler, K. Redlich, S. Wheaton, Comparison of chemical freeze-out criteria in heavy-ion collisions, *Phys. Rev. C* 73 (2006) 034905. [arXiv:hep-ph/0511094](https://arxiv.org/abs/hep-ph/0511094), doi:10.1103/PhysRevC.73.034905.

18. J. Manninen, F. Becattini, Chemical freeze-out in ultra-relativistic heavy ion collisions at $s(\text{NN})^{**}(1/2) = 130$ and 200-GeV, *Phys. Rev. C* 78 (2008) 054901. [arXiv:0806.4100](https://arxiv.org/abs/0806.4100), doi:10.1103/PhysRevC.78.054901.
19. J. Cleymans, S. Kabana, I. Kraus, H. Oeschler, K. Redlich, N. Sharma, Antimatter production in proton-proton and heavy-ion collisions at ultrarelativistic energies, *Phys. Rev. C* 84 (2011) 054916. [arXiv:1105.3719](https://arxiv.org/abs/1105.3719), doi:10.1103/PhysRevC.84.054916.
20. A. Andronic, P. Braun-Munzinger, J. Stachel, The Horn, the hadron mass spectrum and the QCD phase diagram: The Statistical model of hadron production in central nucleus-nucleus collisions, *Nucl. Phys. A* 834 (2010) 237C–240C. [arXiv:0911.4931](https://arxiv.org/abs/0911.4931), doi:10.1016/j.nuclphysa.2009.12.048.
21. Identified charged hadron production in Au+Au collisions at $\sqrt{s_{\text{NN}}} = 54.4$ GeV with the STAR detector (12 2025). [arXiv:2512.06415](https://arxiv.org/abs/2512.06415).
22. N. Sharma, L. Kumar, P. M. Lo, K. Redlich, Light-nuclei production in pp and pA collisions in the baryon canonical ensemble approach, *Phys. Rev. C* 107 (5) (2023) 054903. [arXiv:2210.15617](https://arxiv.org/abs/2210.15617), doi:10.1103/PhysRevC.107.054903.